Chemical Engineering Journal 157 (2010) 520–529

Contents lists available at ScienceDirect

Chemical Engineering Journal

journal homepage: www.elsevier.com/locate/cej

Enhancement of methanol production in a novel cascading fluidized-bed hydrogen permselective membrane methanol reactor

M.R. Rahimpour*, M. Bayat, F. Rahmani

School of Chemical and Petroleum Engineering, Department of Chemical Engineering, Shiraz University, Shiraz 71345, Iran

ARTICLE INFO

Article history:
Received 6 September 2009
Received in revised form
22 December 2009
Accepted 24 December 2009

Keywords:
Cascading fluidized-bed membrane reactor
Methanol synthesis
Pd–Ag membrane

ABSTRACT

In this work, a novel cascading fluidized-bed hydrogen permselective membrane methanol reactor (CFB-MMR) concept has been proposed. In the first catalyst bed, the synthesis gas is partly converted to methanol in water-cooled reactor which is a fluidized-bed. In the second bed which is a membrane assisted fluidized-bed reactor, the reaction heat is used to preheat the feed gas to the first bed. This reactor configuration solves some observed drawbacks of new conventional dual-type methanol reactor even better than fluidized-bed membrane dual-type methanol reactor (FBMDMR). The two-phase theory in bubbling regime of fluidization is used to model and simulate the proposed reactor. The proposed model has been used to compare the performance of a CFBMMR with industrial dual-type methanol reactor (IDMR) and FBMDMR. This comparison shows that fluidizing catalyst bed in the water-cooled reactor caused a favourable temperature profile along the CFBMMR. Additionally, the simulation results represent 3.94% and 9.53% enhancement in the yield of methanol production in comparison with FBMDMR and IDMR respectively.

1. Introduction

Methanol is an important industrial chemical that will play a major role in the energy sector, where it could provide a convenient hydrogen source for fuel cells, or serve as intermediate for synthetic fuels such as dimethyl ether (DME) [1] and as a raw material for the production of chemicals such as formaldehyde and acetic acid. Methanol synthesis is the second largest present use of hydrogen, after ammonia synthesis and is produced by catalytic conversion of synthesis gas (H_2, CO_2, and CO) [2]. Improvement in production efficiency of important chemicals by only a few percents can sometimes result in significant profit increases, energy conservation and environmental protection, especially for a chemical such as methanol which is produced in a worldwide range [3].

The factors affecting the production rate in industrial methanol synthesis are parameters such as thermodynamic equilibrium limitations and catalyst deactivation and variation in the composition of the reacting gas. Also diffusional limitations due to relatively large catalyst particles cannot be eliminated in fixed-bed configurations by usage of smaller particles because pressure drop in the reactor is increased.

1.1. Process and model

The importance of methanol has motivated numerous studies whose aim was to improve the efficiency of industrial methanol synthesis reactor. Dynamic simulation of conventional methanol synthesis reactor was investigated by Lovik et al. [4] for long-term optimization. Rahimpour et al. [5] studied deactivation of methanol synthesis catalyst and proposed the mechanisms for deactivation of this type of catalyst. Velardi and Barresi [6] proposed a multi-stage methanol reactor network with auto-thermal behaviour to promote the reactor performance. Rahimpour [7] proposed a two-stage catalyst bed concept for the conversion of carbon dioxide into methanol. Rahimpour et al. [8,9] have studied a comparison of dual-type and conventional methanol synthesis reactor in the presence of catalyst deactivation. Struis et al. [10] have considered increasing in methanol yield by using membrane reactor. Gallucci et al. [11] have shown that using a membrane reactor is possible to obtain higher conversion of CO_2 and both higher methanol selectivity and methanol yield with respect to a traditional reactor. Rahimpour et al. [12] have investigated the enhancement of methanol production in membrane dual-type reactor. Elnashaie and Wagialla [13] have studied the fluidized-bed reactor concept for methanol synthesis. Rahimpour et al. [14] have investigated the enhancement of methanol production in a novel fluidized-bed membrane dual-type reactor for methanol synthesis. Rahimpour et al. [15] have considered the enhancement of methanol production in a novel fluidized-bed hydrogen permselective membrane reac-

* Corresponding author. Tel.: +98 711 2303071; fax: +98 711 6287294.
E-mail address: rahimpor@shirazu.ac.ir (M.R. Rahimpour).

1385-8947/$ – see front matter © 2010 Elsevier B.V. All rights reserved.
doi:10.1016/j.cej.2009.12.048

Nomenclature

A_c	cross-section area of each tube (m^2)
Ar	Archimedes number
A_{shell}	cross-section area of shell (m^2)
a_b	specific surface area of bubble ($m^2\,m^{-3}$)
a_v	specific surface area of catalyst pellet ($m^2\,m^{-3}$)
C_{Pg}	specific heat of the gas at constant pressure ($J\,mol^{-1}\,K^{-1}$)
C_{ph}	specific heat of the hydrogen at constant pressure ($J\,mol^{-1}\,K^{-1}$)
C_{Ps}	specific heat of the catalyst at constant pressure ($J\,mol^{-1}\,K^{-1}$)
c_t	total concentration ($mol\,m^{-3}$)
d_p	particle diameter (m)
d_b	bubble diameter (m)
F^{sh}	total molar flow in shell side ($mol\,s^{-1}$)
F^t	total molar flow per tube ($mol\,s^{-1}$)
F^e	molar flow in emulsion side ($mol\,s^{-1}$)
F^b	molar flow in bubble side ($mol\,s^{-1}$)
K_{bei}	mass transfer coefficient for component i in fluidized-bed ($m\,s^{-1}$)
k_{gi}	mass transfer coefficient for component i ($m\,s^{-1}$)
P_a	atmospheric pressure (bar)
P_H^t	tube side pressure (bar)
P_H^{sh}	shell side pressure (bar)
$\bar{P}$	permeability of hydrogen through Pd–Ag layer ($mol\,m^{-1}\,s^{-1}\,Pa^{-1/2}$)
P_0	pre-exponential factor of hydrogen permeability ($mol\,m^{-1}\,s^{-1}\,Pa^{-1}$)
R_i	inner radius of Pd–Ag layer (m)
R_o	outer radius of Pd–Ag layer (m)
r_i	reaction rate of component i ($mol\,kg^{-1}\,s^{-1}$)
T	bulk gas phase temperature (K)
T_R	reference temperature used in the deactivation model (K)
T_s	temperature of solid phase (K)
T_{sat}	saturated temperature of boiling water at operating pressure (K)
T_{shell}	temperature of coolant stream, in first reactor (K)
T_{tube}	temperature of coolant stream, in second reactor (K)
U_{shell}	overall heat transfer coefficient between coolant and process streams ($W\,m^{-2}\,K^{-1}$)
u_g	linear velocity of fluid phase ($m\,s^{-1}$)
u_b	velocity of rise of bubbles ($m\,s^{-1}$)
u_e	linear velocity of emulsion phase ($m\,s^{-1}$)
y_i	mole fraction of component i in the fluid phase ($mol\,mol^{-1}$)
y_{is}	mole fraction of component i in the solid phase ($mol\,mol^{-1}$)
y_i^b	mole fraction of component i in the bubble phase ($mol\,mol^{-1}$)
y_i^e	mole fraction of component i in the emulsion phase ($mol\,mol^{-1}$)
Z	axial reactor coordinate (m)

Greek letters

α_H	hydrogen permeation rate constant ($mol\,m^{-1}\,s^{-1}\,Pa^{-1/2}$)
$\Delta H_{f,i}$	enthalpy of formation of component i ($J\,mol^{-1}$)
ΔH_{298}	enthalpy of reaction at 298 K ($J\,mol^{-1}$)
ε_B	void fraction of catalytic bed
ε_s	void fraction of catalyst
ε_{mf}	void fraction of catalytic bed at minimum fluidization
ε_w	void fraction of bed next to the wall of the tube
ν	stoichiometric coefficient
ν_{ci}	critical volume of component i ($cm^3\,mol^{-1}$)
ρ	density of fluid phase ($kg\,m^{-3}$)
ρ_B	density of catalytic bed ($kg\,m^{-3}$)
ρ_s	density of catalyst ($kg\,m^{-3}$)
η	catalyst effectiveness factor
δ	bubble phase volume as a fraction of total bed volume

Superscripts and subscripts

i	component i
f	feed conditions
in	inlet conditions
out	outlet conditions
s	at catalyst surface
sh	shell side
T	tube side
b	bubble phase
e	emulsion phase
mf	minimum fluidization

tor in the presence of catalyst deactivation. Recently, a dual-type reactor system instead of a single-type reactor was developed for methanol synthesis. The dual-type methanol reactor is an advanced technology for converting natural gas to methanol at low cost and in large quantities. This system is mainly based on the two-stage reactor system consisting of a water-cooled and a gas-cooled reactor. The synthesis gas is fed to the tubes of the gas-cooled reactor (second reactor). This cold feed synthesis gas is routed through tubes of the second reactor in a counter-current flow with reacting gas and heated by heat of reaction produced in the shell. So, the reacting gas temperature is continuously reduced over the reaction path in the second reactor. The outlet synthesis gas from the second reactor is fed to tubes of the first reactor (water-cooled) and the chemical reaction is initiated by catalyst. The heat of reaction is transferred to the cooling water inside the shell of reactor. In this stage, the synthesis gas is partly converted to methanol in a water-cooled single-type reactor. The methanol-containing gas leaving the first reactor is directed into the shell of the second reactor. Finally, the product is removed from the downstream of the second reactor [16]. The operating data of this conventional reactor shows high pressure drop, plug in and low performance of gas-cooled reactor in comparison with water-cooled reactor [16]. As mentioned above, the reactions in the gas-cooled reactor are taking place in a large diameter reactor (shell side) so that radial gradient of concentration and temperature prevent higher performance of this reactor. One potentially interesting idea for this type of reactor is using a fluidized-bed concept instead of a packed-bed reactor in both reactors (gas-cooled and water-cooled reactors) which is the subject of this work. Conventional packed-bed reactors are seriously limited by poor heat transfer and low catalyst particle effectiveness factors because of severe diffusional limitations with the catalyst particle sizes used [17]. Smaller particle sizes are infeasible in packed-bed systems because of pressure drop considerations [18]. The advantages of the new proposed concept are a small pressure drop, prevention of problems such as radial gradients, plug in and internal mass transfer limitation, and, if desired, a high production capacity. In addition, using fluidized-bed concept provides a uniform temperature along the reactor because of the absence of radial and axial temperature gradients which prolong the service life of the catalyst and prevents higher damage to the membrane wall of the gas-cooled reactor. Furthermore, it can oper-

ate with much lower pressure drop than packed-beds while very small catalyst particles can be used [19]. Although fluidized-bed reactor has some advantages, there are some possible disadvantages using fluidized-bed reactor as follows: difficulties in reactor construction and membrane sealing, erosion of reactor internals and catalyst attrition [20].

1.2. Pd–Ag membrane

As a solution to overcome the thermodynamic limitations, reactor operation with the addition of H_2 to the reacting gas by using membrane can be devised using permselective membranes that shift the reaction equilibrium in a favourable direction [21–23] as well as thermal uniformity, offered by fluidized-bed systems, is advantageous for maximizing membrane utilization and for minimizing thermal stresses in the membranes [24]. The applications of membrane reaction technology in chemical reaction processes are now mainly focused on reaction systems containing hydrogen and oxygen, and are based on inorganic membranes such as Pd and ceramic membranes [25]. In many hydrogen-related reaction systems, Pd-alloy membranes on a stainless steel support were used as the hydrogen permeable membrane [26]. Abate et al. have measured the permeation behaviour of the membrane with pure H_2 at three different temperatures in the 350–450 °C range. A stable behaviour is typically observed after few hours, but in some cases the time of the test was extended to have better indications on stability of operations [27].

For improving the longevity of the palladium membranes, which are sensible in the face of heating and hydrogen, Palladium–silver (Pd–Ag) alloy is used [28]. Toshishige and Suzuki showed that the durability of the alloy membrane (Ag > 20%) by cyclic change of gas and temperature was improved and it was demonstrated to prevent lattice expansion by alloying with more than 20% of silver [29]. Alloying the palladium, especially with silver, reduces the critical temperature for embitterment and leads to an increase in the hydrogen permeability. The highest hydrogen permeability was observed at an alloy composition of 23 wt% silver [30]. The Pd–Ag membrane is single phase after annealing in H_2 at 400 and 500 °C and it was reported that hydrogen permeation rate increases in a single phase Pd–Ag alloy [31].

Palladium-based membranes have been used for decades in hydrogen extraction because of their high permeability and good surface properties and because palladium, like all metals, is 100% selective for hydrogen transport [32]. These membranes combine excellent hydrogen transport and discrimination properties with resistance to high temperatures, corrosion, and solvents. Key requirements for the successful development of palladium-based membranes are low costs as well as permselectivity combined with good mechanical, thermal and long-term stability [33]. These properties make palladium-based membranes such as Pd–Ag membranes very attractive for use with petrochemical gases.

1.3. Objectives

In this paper, two-phase bubbling model for both reactors was developed to analyze the performance of cascading fluidized-bed membrane reactor. Moreover, we aim to demonstrate the advantages of the fluidized-bed concept in both reactor and the viability of this new configuration using theoretical investigation. In order to have a realistic comparison with industrial dual-type methanol reactor and fluidized-bed membrane dual-type methanol reactor, the same operating conditions of an actual IDMR are used to simulate the performance of the suggested CFBMMR. The results show that the methanol production rate in CFBMMR is greater than in IDMR and even in FBMDMR.

Table 1
Catalyst and specifications of both reactors of IDMR [16].

Water-cooled reactor		Gas-cooled reactor	
Parameter	Value	Value	Unit
D	4.5	5.5	m
D_i	40.3	21.2	mm
D_o	4.5	25.4	mm
d_p	0.00574	0.00574	m
ρ_s	1770	1770	kg m^{-3}
C_{Ps}	5.0	5.0	kJ kg^{-1} K^{-1}
λ_c	0.004	0.004	W m^{-1} K^{-1}
a_v	625.7	625.7	m^2 m^{-3}
ε_s	0.39	0.39	–
ε_B	0.39	0.39	–
Tube length	8	10	m
Number of tubes	5955	3026	–
Shell side pressure	–	71.2	bar
Tube side pressure	75	76.98	bar

2. Process description

2.1. Industrial dual-type methanol reactor (IDMR)

The schematic diagram of industrial dual-type methanol reactor is presented in Fig. 1. The catalyst is packed in vertical tubes of first reactor and shell side of second reactor. The methanol synthesis reactions are carried out over commercial $CuO/ZnO/Al_2O_3$ catalyst. The technical design data of the catalyst pellet and input data of IDMR are summarized in Tables 1 and 2. This system is mainly based on the two-stage reactor system consisting of a water-cooled and a gas-cooled reactor. The cold feed synthesis gas is fed to the tubes of the gas-cooled reactor (second reactor) from bottom of reactor and flowing in counter-current mode with reacting gas mixture in the shell of the reactor. Then the synthesis gas is heated by the heat of reaction produced in the shell. Therefore, the reacting gas temperature is continuously reduced through the reaction path in the second reactor. The outlet synthesis gas from the second reactor is fed to tubes of the first reactor (water-cooled) and the chemical reaction is initiated by the catalyst. The heat of reaction is transferred to the cooling water inside the shell of reactor. In the first stage, methanol is partly produced.

The gas leaving the first reactor is directed into the shell of the second reactor from top of the reactor. Finally, the product is removed from the downstream of the second reactor (gas-cooled reactor). As fresh synthesis gas is only fed to the first reactor, no catalyst poisons reach the second reactor.

2.2. Cascading fluidized-bed membrane methanol reactor (CFBMMR)

Fig. 2 shows the schematic diagram of a CFBMMR configuration. Basically, the process in CFBMMR is similar to IDMR with the excep-

Table 2
Input data of the IDMR [16].

Feed conditions	Value
Feed composition (mol%)	
CO_2	8.49
CO	8.68
H_2	64.61
CH_4	9.47
N_2	8.2
H_2O	0.1
CH_3OH	0.37
Argon	0.24
Inlet temperature [K]	401
Pressure [bar]	76

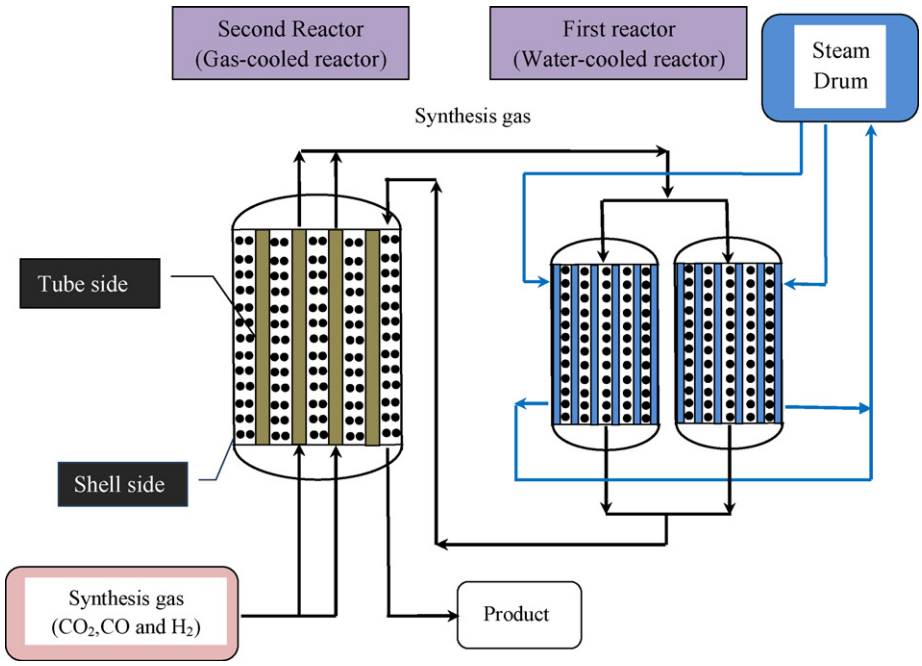

Fig. 1. A schematic diagram of industrial dual-type methanol reactor (IDMR).

tion of some changes. These changes in the new proposed system are as follows:

Firstly, the fixed catalyst bed of the first reactor and second reactor in reaction side has been changed to fluidized-bed by applying small catalyst size. Secondly, in order to fluidize catalyst bed, the reacting gas leaving first reactor is routed to the bottom of the second reactor and also the outlet synthesis gas from the second reactor is fed to the bottom of tubes in the first reactor (water-cooled). Thirdly, the walls of tubes in the second reactor (gas-cooled reactor) consist of hydrogen permselective membrane. The pressure difference between the shell (71.2 bars) and tube (76.98 bars) sides in IDMR is the driving force for the diffusion of hydrogen through the Pd–Ag membrane layer. On the other hand, in the new system, the mass and heat transfer process simultaneously occurs between shell and tube, while in the industrial-type system only a heat transfer occurs. This simulation study is based on a Pd–Ag layer thickness of 1.1 μm.

3. Mathematical model

3.1. IDMR model

3.1.1. Water-cooled reactor (first reactor)

The mathematical model for the simulation of first reactor in IDMR was developed based on the following assumptions:

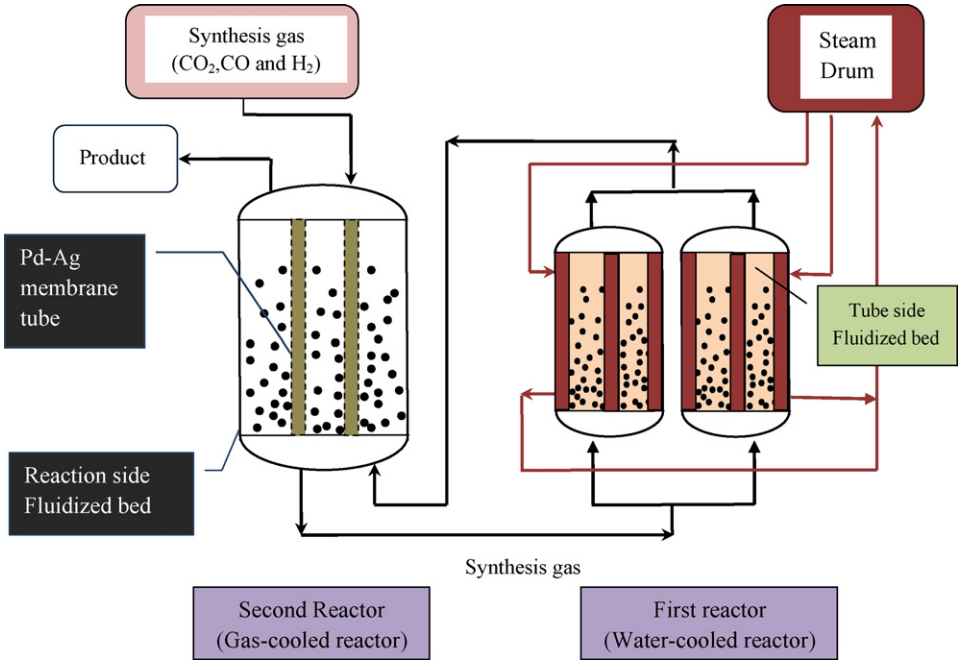

Fig. 2. A schematic diagram of cascading fluidized-bed membrane methanol reactor (CFBMMR).

(1) One-dimensional plug flow in shell and tube sides; (2) axial dispersion of heat is negligible compared to convection; (3) gases are ideal; (4) the radial diffusion in catalyst pellet is neglected. The mass and energy balance for solid phase is expressed by:

$$k_{g_i} \cdot c_t \cdot a_v \cdot (y_i - y_{is}) + \eta \cdot r_i \rho_B = 0, \quad i = 1, 2, \ldots, N \tag{1}$$

$$a_v h_f (T - T_s) + \rho_B \cdot \sum_{i=1}^{N} \eta \cdot r_i (-\Delta H_{f,i}) = 0 \tag{2}$$

where y_{is} and T_s are the mole fraction and temperature of solid phase respectively, and i represents H_2, CO_2, CO, CH_3OH, H_2O, argon, nitrogen and methane.

η is the effectiveness factor of catalyst and is calculated according to procedure explained by Rezaie et al. [34]. Moreover the kinetic model and the equilibrium rate constants are selected from Graaf's studies [35,36].

The following two conservation equations are written for the fluid phase:

$$-\frac{F_t}{A_c}\frac{dy_i}{dz} + a_v c_t k_{g_i}(y_{is} - y_i) = 0, \quad i = 1, 2, \ldots, N \tag{3}$$

$$-\frac{F_t}{A_c} c_{pg} \frac{dT}{dz} + a_v h_f (T_s - T) + \frac{\pi D_i}{A_c} U_{shell}(T_{shell} - T) = 0 \tag{4}$$

where y_i and T are the fluid phase mole fraction and temperature, respectively. As can be seen in Fig. 2, the outlet synthesis gas from the second reactor is the inlet synthesis gas to the first reactor. The boundary conditions are unknown and the more details are explained as numerical solution in steady-state computations.

$$z = 0; \qquad y_i = y_{i_{in}}; \qquad T = T_{in} \tag{5}$$

3.1.2. Gas-cooled reactor (second reactor)

3.1.2.1. Shell side (reaction side). The mass and energy balance for solid phase in the gas-cooled reactor is the same as that in the water-cooled reactor. The following equations are written for fluid phase:

$$-\frac{F^{sh}}{A_{shell}}\frac{dy_i}{dz} + a_v c_t k_{g_i}(y_{is} - y_i) = 0, \quad i = 1, 2, \ldots, N \tag{6}$$

$$-\frac{F^{sh}}{A_{shell}} C_{pg} \frac{dT}{dz} + a_v h_f (T_s - T) + \frac{\pi D_i}{A_{shell}} U_{tube}(T_{tube} - T) = 0 \tag{7}$$

3.1.2.2. Tube side (feed synthesis gas flow). The energy balance equation for fluid phase is given:

$$\frac{F^t}{A_c} C_{pg} \frac{dT_{tube}}{dz} + \frac{\pi D_i}{A_c} U_{tube}(T - T_{tube}) = 0 \tag{8}$$

where F^t is the molar flow rate. The boundary conditions are as follows:

$$z = L; \qquad y_i = y_{if}; \qquad T = T_f \tag{9}$$

3.2. CFBMMR model

3.2.1. Water-cooled reactor (first reactor)

The mathematical simulation for first and second reactor of CFB-MMR was developed based on the following assumptions:

(1) Ideal gas behaviour is assumed; (2) reactions mostly occur in emulsion phase; (3) in view of their small size, the diffusional resistance inside the catalyst particles is neglected; (4) the dense catalyst bed is considered to be composed of bubble phase and emulsion phase; (5) bubbles are assumed to be spherical; (6) the bubble phase contains some catalyst particles, which involve in reactions but the extend of reaction in bubble phase is much less than emulsion phase; (7) due to rapid mixing, the operation is assumed to be isothermal which means bubble and emulsion phases have same temperature; (8) the top 3 m of both reactors is freeboard region which is devoid of catalyst and no changes occur in this region. We consider an element of length dz as depicted in Fig. 3.

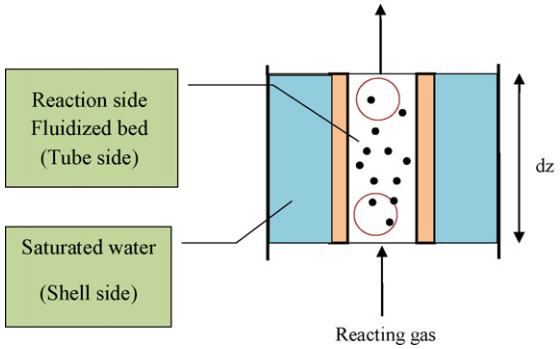

Fig. 3. Schematic diagram of an elemental volume of first reactor.

The resulting mass balances for bubble and emulsion phase are given in Eqs. (10) and (11).

Bubble phase:

$$\delta K_{bei} c_t a_b (y_{ie} - y_{ib}) - \frac{\delta}{A_c}\frac{dF_i^b}{dz} + \delta \cdot \gamma \cdot \rho_s \sum_{j=1}^{3} r_{bij} = 0, \quad i = 1, 2, \ldots, N \tag{10}$$

where K_{bei} is the mass transfer coefficient between bubble phase and emulsion phase, y_{ie} and y_{ib} are the emulsion phase and bubble phase mole fraction, respectively and γ is the volume fraction of catalyst bed occupied by solid particles in bubble phase.

Emulsion phase:

$$\delta K_{bei} c_t a_b (y_{ib} - y_{ie}) - \frac{1-\delta}{Ac}\frac{dF_i^e}{dz} + (1-\delta)\rho_e \cdot \eta \cdot \sum_{j=1}^{3} r_{ij} = 0 \tag{11}$$

where F_i^b and F_i^e are given as follows:

$$F_i^b = y_{ib} F^t; \qquad F_i^e = y_{ie} F^t \tag{12}$$

The heat transfer equation between bed (tubes) and shell side (cooling water):

$$\frac{\pi D_i}{A_{sh}} U_{tube}(T_{shell} - T) + (1-\delta)\rho_e \cdot \eta \cdot a \cdot \sum_{j=1}^{3} r_j (-\Delta H_{f,j}) + \delta \cdot \gamma \cdot \rho_B \cdot \eta \cdot a \cdot \sum_{j=1}^{3} r_{bj} (-\Delta H_{f,j}) = 0 \tag{13}$$

where T_{shell} is temperature in shell side which is constant and A_{sh} is the equivalent area around each tube [37].

3.2.2. Gas-cooled reactor (second reactor)

3.2.2.1. Shell side (reaction side). The assumptions considered for the first reactor are also valid in the gas-cooled reactor. Moreover in the second reactor was assumed: (1) hydrogen is the only species which permeates through the membrane tube walls; (2) hydrogen permeates to the emulsion phase; (3) the axial diffusion of hydrogen through the membrane is neglected compared to the radial diffusion; We consider an element of length dz as depicted in Fig. 4.

The resulting mass balances for bubble and emulsion phase are given in Eqs. (14) and (15).

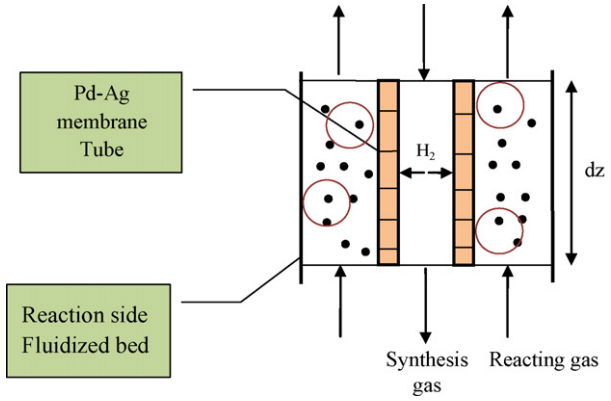

Fig. 4. Schematic diagram of an elemental volume of second reactor.

Bubble phase:

$$\delta K_{bei} c_t a_b (y_{ie} - y_{ib}) - \frac{\delta}{A_{shell}} \frac{dF_I^b}{dz} + \delta \cdot \gamma \cdot \rho_s \sum_{j=1}^{3} r_{bij} = 0,$$

$$i = 1, 2, \ldots, N \tag{14}$$

where K_{bei} is the mass transfer coefficient between bubble phase and emulsion phase, y_{ie} and y_{ib} are the emulsion phase and bubble phase mole fraction, respectively and γ is the volume fraction of catalyst bed occupied by solid particles in bubble phase.

Emulsion phase:

$$\delta K_{bei} c_t a_b (y_{ib} - y_{ie}) - \frac{1-\delta}{A_{shell}} \frac{dF_i^e}{dz} + (1-\delta)\rho_e \cdot \eta \cdot \sum_{j=1}^{3} r_{ij} + (1-\delta)\frac{\alpha_H}{A_s}(\sqrt{P_H^t} - \sqrt{P_H^s}) = 0 \tag{15}$$

where α_H is hydrogen permeation rate constant, P_H^t and P_H^{sh} are hydrogen partial pressures in tube and reaction side (shell side), respectively. F_i^b and F_i^e are given as follows:

$$F_i^b = y_{ib} F^{sh}; \qquad F_i^e = y_{ie} F^{sh} \tag{16}$$

The heat transfer equation between bed and tubes:

$$-(1-\delta)\frac{\alpha_H}{A_s}(\sqrt{p_H^r} - \sqrt{p_H^s})C_{ph}(T - T_{tube}) + \frac{\pi D_i}{A_{sh}} U_{shell}(T_{tube} - T) + (1-\delta)\cdot\eta\cdot\rho_e \sum_{j=1}^{3} r_j(-\Delta H_{f,j}) + \delta\cdot\gamma\cdot\rho_B\cdot\eta\sum_{j=1}^{3} r_{bj}(-\Delta H_{f,j}) = 0 \tag{17}$$

where T_{tube} is temperature in tube side and A_{sh} is the equivalent area around each tube [37].

3.2.2.2. Tube side (fresh feed synthesis gas flow). The mass and energy balance equations for fluid phase are given as follows:

$$\frac{F^t}{A_c}\frac{dy_i}{dz} - \frac{\alpha_H}{A_s}(\sqrt{P_H^t} - \sqrt{P_H^s}) = 0, \quad i = 1, 2, \ldots, N \tag{18}$$

$$\frac{F^t}{A_c} C_{pg} \frac{dT_{tube}}{dz} + \frac{\alpha_H}{A_s}(\sqrt{P_H^t} - \sqrt{P_H^s})C_{ph}(T - T_{tube}) + \frac{\pi D_i}{A_c} U_{tube}(T - T_{tube}) = 0 \tag{19}$$

Table 3
Hydrodynamic parameters [40–43].

Parameter	Equation
Superficial velocity at minimum fluidization	$\frac{1.75}{\varepsilon_{mf}^3 \varphi_s}\left[\frac{d_p \rho_g u_{mf}}{\mu}\right]^2 + \frac{150(1-\varepsilon_{mf})}{\varepsilon_{mf}^3 \varphi_s}\left[\frac{d_p \rho_g u_{mf}}{\mu}\right] = Ar$
Archimedes number	$Ar = \frac{d_p^3 \rho_g (\rho_p - \rho_g) g}{\mu^2}$
Bed voidage at minimum fluidization velocity	$\varepsilon_{mf} = 0.586 Ar^{-0.029}\left(\frac{\rho_g}{\rho_p}\right)^{0.021}$
Bubble diameter	$d_b = d_{bm} - (d_{bm} - d_{bo})\exp\left(\frac{-0.3z}{D}\right)$ $d_{bm} = 0.65\left[\frac{\pi}{4}D^2(u_o - u_{mf})\right]^{0.4}$ $d_{bo} = 0.376(u_o - u_{mf})^2$
Mass transfer coefficient (bubble-emulsion phase)	$K_{bei} = \frac{u_{mf}}{3} + \left(\frac{4 D_{jm} \varepsilon_{mf} u_b}{\pi d_b}\right)^{1/2}$
Bubble rising velocity	$u_b = u - u_{mf} + 0.711\sqrt{g d_b}$
Specific surface area for bubble	$\delta = \frac{u - u_{mf}}{u_b}$
Volume fraction of bubble phase to overall bed	$a_b = \frac{6\delta}{d_b}$
Density for emulsion phase	$\rho_e = \rho_p\left(1 - \varepsilon_{mf}\right)$

where F^t is molar flow rate and T_{tube} is temperature of synthesis gas in tube side. The boundary conditions are as follows:

$$z = L; \qquad y_i = y_{if}; \qquad T = T_f \tag{20}$$

The hydrodynamic parameters for CFBMMR system have been taken from the literature (summarized in Table 3) although these correlations were originally obtained for beds without internals. It is assumed that these correlations can reasonably well describe the FBMR (see Table 3). For an explanation of the symbols used, the reader is referred to Notations section.

3.2.3. Hydrogen permeation in the Pd–Ag membrane

The flux of hydrogen permeating through the palladium membrane, j, will depends on the difference in the hydrogen partial pressure on the two sides of the membrane. Here, the hydrogen permeation is determined assuming Sieverts' law:

$$j_H = \alpha_H(\sqrt{P_H^t} - \sqrt{P_H^s}) \tag{21}$$

Data for the permeation of hydrogen through Pd–Ag membrane were determined experimentally by Hara et al. [38]. In Eqs. (8)–(13), α_H is hydrogen permeation rate constant and is defined as [38]:

$$\alpha_H = \frac{2\pi L \bar{P}}{\ln(R_o/R_i)} \tag{22}$$

where R_o and R_i stand for outer and inner radius of Pd–Ag layer. Here, the hydrogen permeability through Pd–Ag layer is determined assuming the Arrhenius law, which as a function of temperature is as follows [39,40]:

$$\bar{P} = P_0 \exp\left(\frac{-E_p}{RT}\right) \tag{23}$$

where the pre-exponential factor P_0 above 200 °C is reported as 6.33×10^{-8} mol m^{-1} s^{-1} Pa$^{-1/2}$ and activation energy E_p is 15.7 kJ kmol^{-1} [39,40].

Table 4
Comparison between the results of model for IDMR with plant data.

Product condition	Plant	Predicted	Error × 100%
Composition (mol%)			
CH_3OH	0.104	0.1023	−3.4
CO_2	0.0709	0.0764	−4.38
CO	0.0251	0.0228	−9.16
H_2O	0.0234	0.0211	−9.82
H_2	0.5519	0.5323	−3.55
N_2/Ar	0.0968	0.0905	−6.5
CH_4	0.114	0.103	−9.64
Temperature [K]	495	489.5	−1.2
CO_2 removal rate [ton/day]	2500	2542.5	1.7

4. Solution of model

The basic structure of the model is consisted of mass conservative rule of bubble and emulsion phase as well as heat transfer equation in the both reactor. These equations have to be coupled with non-linear algebraic equations of the kinetic model and also fluidized-bed hydrodynamic and transport property correlation and other auxiliary correlations.

In order to solve the set of reactor model equations (the set of non-linear differential-algebraic equations) at the steady-state condition, backward finite difference approximation was applied to the system of ordinary differential-algebraic equations. The set of non-linear algebraic equations has been solved using the shooting method. In fact, the temperature (T_{in}) and H_2 mole fraction (y_{in}) of inlet feed synthesis gas for water-cooled reactor are unknown, while the temperature (T_f) and H_2 mole fraction (y_f) of feed synthesis gas stream are known. The shooting method converts the boundary value problem to an initial value one. The solution is possible by guessing a value for T_{in} and y_{in} of heated feed synthesis gas to the water-cooled reactor. The water-cooled and gas-cooled reactors are divided into 14 and 16 sections, respectively and then Gauss–Newton method is used to solve the non-linear algebraic equations in each section. At the end, the calculated values of temperature (T_f) and H_2 mole fraction (y_f) of fresh feed synthesis gas stream are compared with the actual values. This procedure is repeated until the specified terminal values are achieved within small convergence criterion.

5. Results and discussion

5.1. Model validation

The validation of proposed model was carried out by comparison of model results with plant data for industrial dual-type methanol reactor under the design specifications and input data tabulated in Tables 1 and 2, respectively. The model results and the corresponding observed data of the plant are presented in Table 4. It was observed that, the model performed satisfactorily well under industrial conditions and a good agreement between plant data and simulation data existed.

Fig. 5(a)–(c) shows the mole fraction profiles of reactants and products along the reactors resulted from simulation of CFBMMR. Since the model consists of four parts (first reactor, second reactor and freeboard zone in first and second reactors) three different slopes can be seen. In these figures, the solid line separates first reactor (water-cooled reactor) from second reactor (gas-cooled reactor) and dash line in last three meters of first reactor and second reactor presents freeboard zone respectively. While there is no change in freeboard zone, a horizontal line is observed for these parts. Fig. 5(a) shows the mole fraction profile of methanol and H_2 along the reactor. Fig. 5(b) and (c) illustrates similar results for other components. As it is observed, hydrogen, CO_2 and CO mole fractions

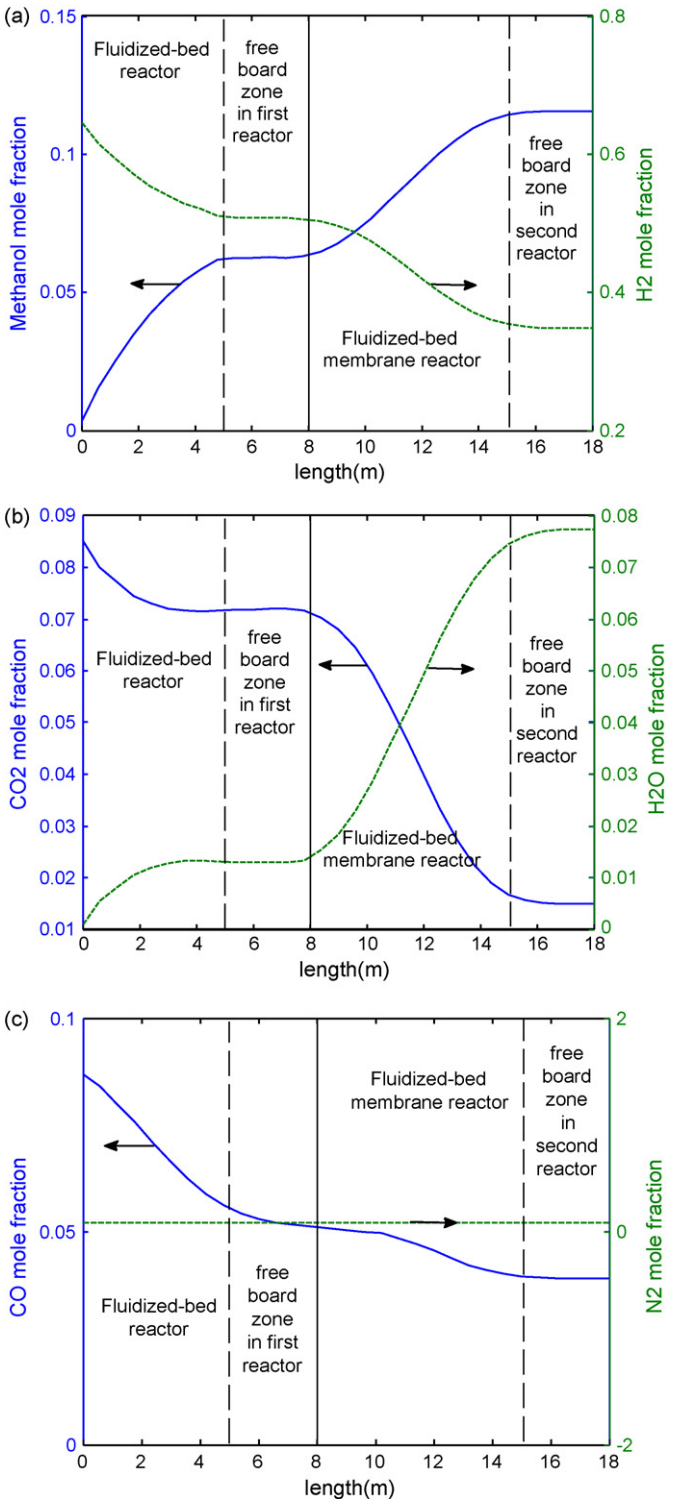

Fig. 5. Mole fraction profiles of (a) methanol and H_2, (b) CO_2 and H_2O and (c) CO and N_2.

decreases as reactant in reactions while methanol and water mole fractions increase along the reactor and nitrogen mole fraction does not change since is inert.

The mole fraction profiles of reactants and products in emulsion and bubble phases along the reactors are presented in Fig. 6. The results were obtained from CFBMMR simulation which attributed to the mass-transport limitations between emulsion and bubble phases. The mole fractions of reactants and products in the emul-

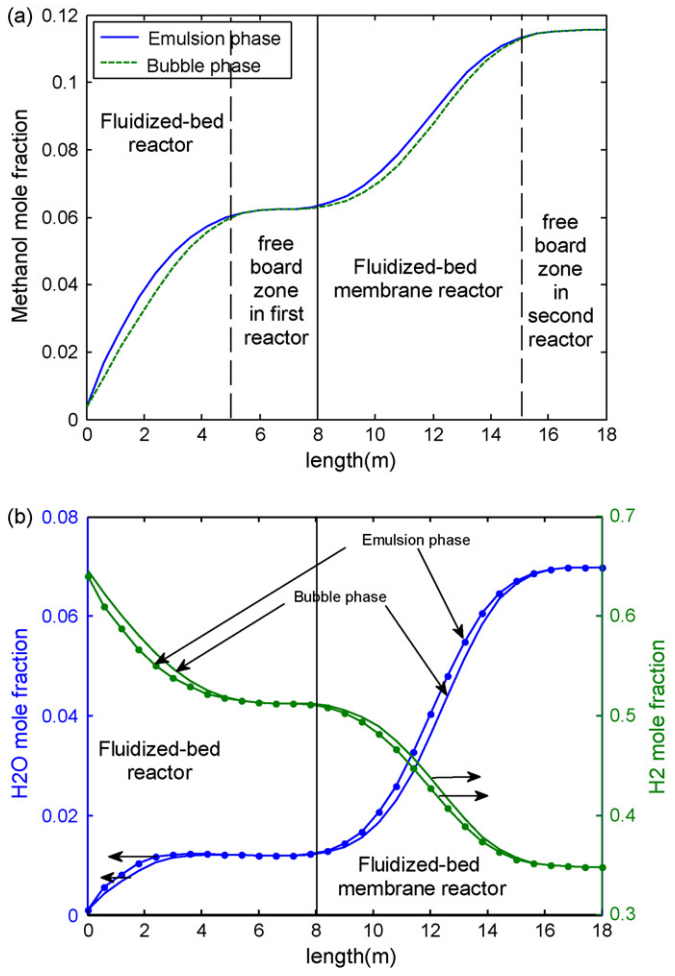

Fig. 6. Mole fractions of emulsion and bubble phases for (a) methanol, (b) H_2O and H_2.

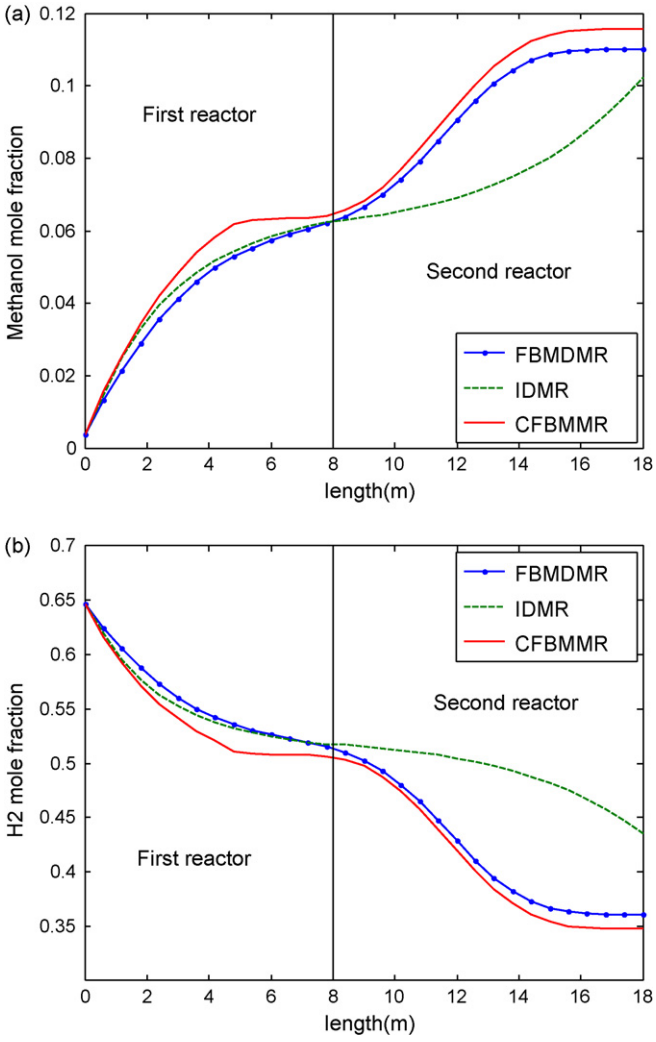

Fig. 7. Comparison of mole fraction profiles for (a) methanol and (b) H_2.

sion phase were lower and higher respectively. This could be explained by the fact that the reaction mostly occurs in the emulsion phase. Consecutively, mole fraction of methanol and H_2O are higher in emulsion phase whereas H_2 mole fraction is lower than bubble phase.

Fig. 7 illustrates the comparison of simulation results for methanol as product and hydrogen as reactant mole fraction for the three types of reactor systems (IDMR, FBMDMR and CFBMMR). In Fig. 7(a), the highest methanol mole fraction is achieved in CFBMMR reactor. Since the FBMDMR and CFBMMR system both have lower pressure drop, overcome mass transfer limitations due to small particle size, they have the higher conversion during the operation. The small difference between CFBMMR and FBMDMR performances is attributed to the positive effect of fluidization of catalyst in the tubes of water-cooled reactor in CFBMMR. Consequently, H_2 consumption rate in CFBMMR and FBMDMR is higher than IDMR; see Fig. 7(b).

The comparison of the hydrogen permeation rate profile along the second reactor of FBMDMR and CFBMMR systems is illustrated in Fig. 8. As can be seen, the permeation rate of hydrogen decreases along the gas-cooled reactor.

Comparison profile for temperature of reacting gas for the three systems is presented in Fig. 9. Generally, feed gas is fed to the tube of the second reactor at 401 K and is heated by using the heat of reaction in the three types of reactor. The outlet synthesis gas temperature is not enough for the initiation of reaction in the first reactor. In this way, there is a need for a heat exchanger in order

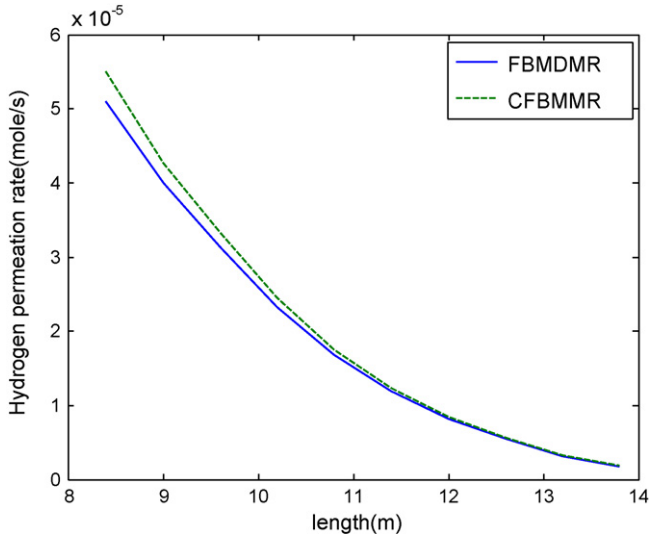

Fig. 8. Comparison of the hydrogen permeation rate profile along the second reactor.

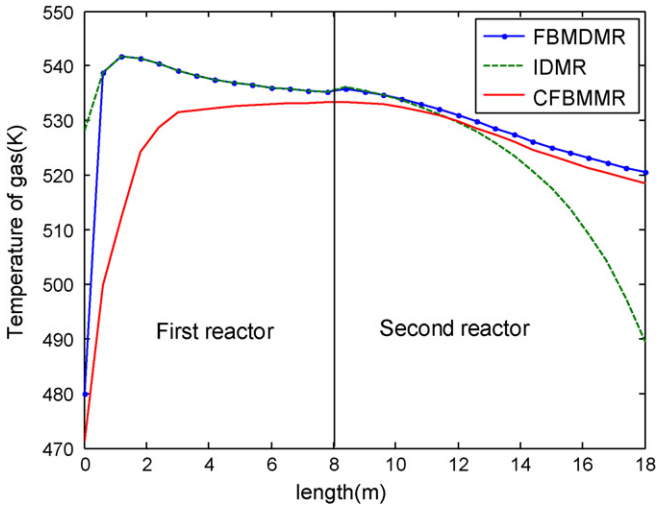

Fig. 9. Comparison profile of gas temperature in the three systems.

to heat the feed gas with outlet product stream. As Fig. 9 shows the temperature of reacting gas in the second reactor is continuously reduced and, in turn the catalysts are exposed to less extreme temperatures and, catalyst deactivation via sintering is reduced.

For exothermic systems such as methanol synthesis thermodynamic equilibrium becomes favourable at lower temperatures. As shown in Fig. 9 the temperature control of the CFBMMR is easier in first reactor. There is not a suddenly rises of temperature for this system at first 2 m of reactor. For simulation purposes, the maximum temperature for the $CuO/ZnO/Al_2O_3$ catalyst to remain active is assumed to be 543 K. As can be seen, in IDMR and FBMDMR systems, the temperature of catalyst bed cannot be controlled (i.e., a hot spot is likely) whereas in CFBMMR is achievable. One of the main advantages of the fluidized-bed reactor is the excellent tube-to-bed heat transfer, which allows a safe and efficient reactor operation even for highly exothermic reactions. The temperature uniformity as a result of very good heat transfer and temperature equalization characteristics of fluidized-bed improves the products distribution [44].

The comparisons of methanol production rate in the three types of reactors are presented in Fig. 10. As can be seen, there is a considerable increase in amount of methanol production in CFBMMR. An increase about 3.94% and 9.53% in methanol yield was observed for cascading fluidized-bed membrane reactor in comparison with FBMDMR and IDMR, respectively. This significant improvement in methanol production rate for CFBMMR is due to overcoming high drop pressure, mass and heat transport limitations as well as shifting the equilibrium by using permselective membrane.

According to the figure, in methanol production point of view this feature suggests that the concept of CFBMMR system is an interesting candidate for application in methanol synthesis. However, from an industrial point of view there are still many issues to be addressed before putting a case for successful commercialization, such as difficulties in reactor construction, the cost of membranes and their sealing in the fluidization conditions.

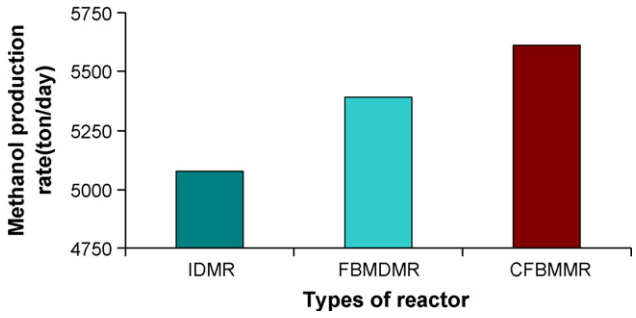

Fig. 10. Comparison of methanol production rate for three types of systems.

6. Conclusion

The methanol synthesis process in the dual-type methanol reactor is limited by the poor heat transfer and low catalyst particle effectiveness factors because of severe diffusional limitations with the catalyst particle sizes used in the packed-bed reactor. Smaller particle sizes are infeasible in packed-bed systems because of pressure drop considerations. Therefore, development of cascading fluidized-bed process and using fluidized-bed concept instead of fixed-bed reactor in the reaction side of both reactors could open the way to increasing the methanol production in the methanol synthesis process. The potential possibilities of the CFBMMR system were analyzed using two-phase bubbling model in the both reactors to obtain the necessary comparative estimates. In this work, the performance of a cascading fluidized-bed membrane methanol reactor (CFBMMR) system was compared with an industrial dual-type methanol reactor and a fluidized-bed membrane dual-type methanol reactor (FBMDMR). This comparison shows a favourable temperature profile along the cascading fluidized-bed hydrogen permselective membrane methanol reactor (CFBMMR). Additionally, the simulation results represent 3.94% and 9.53% enhancement in the yield of methanol production in comparison with FBMDMR and IDMR respectively.

References

[1] T.A. Semelsberger, R.L. Borup, H.L. Greene, Dimethyl ether (DME) as an alternative fuel, J. Power Sources 156 (2006) 497–511.
[2] G.C. Chinchen, P.J. Denny, J.R. Jennings, M.S. Spencer, K.C. Waugh, Synthesis of methanol. Part 1. Catalysts and kinetics, Appl. Catal. 36 (1988) 65.
[3] C.J. Schack, M.A. Mcneil, R.G. Rinker, Methanol synthesis from hydrogen, carbon monoxide, and carbon dioxide over a $Cuo/ZnO/Al_2O_3$ catalyst. I. steady-state kinetics experiments, Appl. Catal. 50 (1989) 247–263.
[4] I. Lovik, M. Hillestad, T. Hertzberg, Long term dynamic optimization of a catalytic reactor system, Comput. Chem. Eng. 22 (1998) 707–710.
[5] M.R. Rahimpour, J. Fathikalajahi, A. Jahanmiri, Selective kinetic deactivation model for methanol synthesis from simultaneous reaction of CO_2 and CO with H_2 on a commercial copper/zinc oxide catalyst, Can. J. Chem. Eng. 76 (1998) 753–760.
[6] S.A. Velardi, A.A. Barresi, Methanol synthesis in a forced unsteady-state reactor network, Chem. Eng. Sci. 57 (2002) 2995–3004.
[7] M.R. Rahimpour, A two-stage catalyst bed concept for conversion of carbon dioxide into methanol, Fuel Process. Technol. 89 (2008) 556–566.
[8] M.R. Rahimpour, M. Lotfinejad, Co-current and counter-current configurations for a membrane dual type methanol reactor, Chem. Eng. Technol. 31 (2008) 38–57.
[9] M.R. Rahimpour, M. Lotfinejad, A comparison of co-current and counter-current modes of operation for a dual type industrial methanol reactor, Chem. Eng. Process. 47 (2008) 1819–1830.
[10] R.P.W.J. Struis, S. Stucki, M. Wiedorn, A membrane reactor for methanol synthesis, J. Membr. Sci. 113 (1996) 93–100.
[11] F. Gallucci, L. Paturzo, A. Basile, An experimental study of CO_2 hydrogenation into methanol involving a zeolite membrane reactor, Chem. Eng. Process. 43 (2004) 1029–1036.
[12] M.R. Rahimpour, M. Lotfinejad, Enhancement of methanol production in a membrane dual-type reactor, Chem. Eng. Technol. 30 (2007) 1062–1076.
[13] K.M. Wagialla, S.S.E.H. Elnashaie, A fluidized bed reactor for methanol synthesis. A theoretical investigation, Ind. Eng. Chem. Res. 30 (1991) 2298–2308.
[14] M.R. Rahimpour, K. Alizadehhesari, A novel fluidized-bed membrane dual type reactor concept for methanol synthesis, Chem. Eng. Technol. 31 (2008) 1–16.
[15] M.R. Rahimpour, H. Elekaei, Enhancement of methanol production in a novel fluidized-bed hydrogen-permselective membrane reactor in the presence of catalyst deactivation, Int. J. Hydrogen Energy 34 (2009) 2208–2223.
[16] Domestic Industrial Methanol Reactor, Design Manual, 2007.
[17] A.M. Adris, S.S.E.H. Elnashaie, R. Hughes, A fluidized bed membrane reactor for the steam reforming of methane, Can. J. Chem. Eng. 69 (1991) 1061–1070.
[18] A. Santos, M. Meneïndez, J. Santamariĭa, Partial oxidation of methane to carbon monoxide and hydrogen in a fluidized bed reactor, Catal. Today 21 (1994) 481–488.

[19] A. Santos, M. Meneĭndez, J. Santamarıĭa, M. Monzon, E.E. Miro, E.A. Lombardo, Oxidation of methane to synthesis gas in a fluidized bed reactor using MgO-based catalysts, J. Catal. 158 (1996) 83–91.
[20] S.A.R.K. Deshmakh, S. Heinrich, L. Morl, M. Van Sint Annaland, J.A.M. Kuipers, Membrane assisted fluidized bed reactors: potentials and hurdles, Chem. Eng. Sci. 62 (2006) 416–436.
[21] A.M. Adris, J.R. Grace, C.J. Lim, S.S.U.S. Elnashaie, Patent 5,326,550, 1994.
[22] A.M. Adris, J.R. Grace, C.J. Lim, The fluidized-bed membrane reactor for steam methane reforming: model verification and parametric study, Chem. Eng. Sci. 52 (1997) 1609–1622.
[23] D.A. Goetsch, G.R. U.S. Say, Patent 4,877,550, 1989.
[24] A.M. Adris, J.R. Grace, Characteristics of fluidized-bed membrane reactors: scale-up and practical issues, Ind. Eng. Chem. Res. 36 (1997) 4549–4556.
[25] M.R. Rahimpour, A. Asgari, Modeling and simulation of ammonia removal from purge gases of ammonia plants using a catalytic Pd–Ag membrane reactor, J. Hazard. Mater. 153 (2008) 557–565.
[26] Y.-M. Lin, M.-H. Rei, Study on the hydrogen production from methanol steam reforming in supported palladium membrane reactor, Catal. Today 67 (2001) 77–84.
[27] S. Abate, Ch. Genovese, S. Perathoner, G. Centi, Performances and stability of a Pd-based supported thin film membrane prepared by EPD with a novel seeding procedure. Part I. Behaviour in H_2:N_2 mixtures, Catal. Today 145 (2009) 63–71.
[28] E.N. Gobina, R. Hughes, D. Monaghan, D. Arnel, High-temperature selective membranes for hydrogen separation, Dev. Chem. Eng. Min. Process. 2 (1994) 105–114.
[29] J. Okazaki, D.A.P. Tanaka, M.A.L. Tanco, Y. Wakui, F. Mizukami, T.M. Suzuki, Hydrogen permeability study of the thin Pd–Ag alloy membranes in the temperature range across the α–β phase transition, J. Membr. Sci. 282 (2006) 370–374.
[30] M.R. Rahimpour, S. Ghader, Theoretical investigation of a Pd-membrane reactor for methanol synthesis, Chem. Eng. Technol. 26 (2003) 902–907.
[31] Y.S. Cheng, K.L. Yeung, Palladium-silver composite membranes by electroless plating technique, J. Membr. Sci. 158 (1999) 127–141.
[32] R.E. Buxbaum, A.B. Kinney, Hydrogen transport through tubular membranes of palladium-coated tantalum and niobium, Ind. Eng. Chem. Res. 35 (1996) 530–537.
[33] R. Dittmeyer, V. Hollein, K. Daub, Membrane reactors for hydrogenation and dehydrogenation processes based on supported palladium, J. Mol. Catal. A: Chem. 173 (2001) 135–184.
[34] N. Rezaie, A. Jahanmiri, B. Moghtaderi, M.R. Rahimpour, A comparison of homogeneous and heterogeneous dynamic models for industrial methanol reactors in the presence of catalyst deactivation, Chem. Eng. Process. 44 (2005) 911–921.
[35] G.H. Graaf, H. Scholtens, E.J. Stamhuis, A.A.C.M. Beenackers, Intra-particle diffusion limitations in low-pressure methanol synthesis, Chem. Eng. Sci. 45 (1990) 773–783.
[36] G.H. Graaf, P.J.J.M. Sijtsema, E.J. Stamhuis, G.E.H. Joosten, Chemical equilibria in methanol synthesis, Chem. Eng. Sci. 41 (1986) 2883–2890.
[37] Z. Chen, Y. Yan, S.S.E.H. Elnashaie, Novel circulating fast fluidized-bed membrane reformer for efficient production of hydrogen from steam reforming of methane, Chem. Eng. Sci. 58 (2003) 4335–4349.
[38] S. Hara, W.C. Xu, K. Sakaki, N. Itoh, Kinetics and hydrogen removal effect for methanol decomposition, Ind. Eng. Chem. Res. 38 (1999) 488–492.
[39] G. Barbieri, F.P.D. Maio, Simulation of the methane steam re-forming process in a catalytic Pd-membrane reactor, Ind. Eng. Chem. Res. 36 (1997) 2121–2127.
[40] G. Shu, B.P.I. Grandjean, S. Kaliaguine, Methane steam reforming in asymmetric Pd- and Pd–Ag/porous SS membrane reactors, Appl. Catal. A 119 (1994) 305–325.
[41] D. Kunii, O. Levenspiel, Fluidization Engineering, Butterworth–Heinemenn, USA, 1991.
[42] S. Mori, C.Y. Wen, Estimation of bubble diameter in gaseous fluidized beds, AIChE J. 21 (1975) 109–115.
[43] J.F. Davidson, D. Harisson, Fluidized Particles, Cambridge Univ. Press, New York, 1963.
[44] M. Alaa-Eldin, Adris, R. John, Grace, Characteristics of fluidized-bed membrane reactors: scale-up and practical issues, Ind. Eng. Chem. Res. 36 (1997) 4549–4556.